Bismuth sulphide-modified molybdenum disulphide as an efficient photocatalyst for hydrogen production under simulated solar light

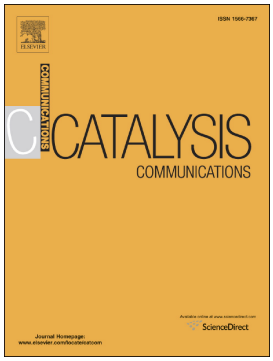

Bismuth sulphide-modified molybdenum disulphide as an efficient photocatalyst for hydrogen production under simulated solar light

W.P. Cathie Lee, Meei-Mei Gui, Lling-Lling Tan, Ta-Yeong Wu, S. Sumathi, Siang-Piao Chai

PII: S1566-7367(17)30187-5
DOI: doi: 10.1016/j.catcom.2017.05.004
Reference: CATCOM 5038

To appear in: *Catalysis Communications*

Received date: 10 January 2017
Revised date: 18 April 2017
Accepted date: 3 May 2017

Please cite this article as: W.P. Cathie Lee, Meei-Mei Gui, Lling-Lling Tan, Ta-Yeong Wu, S. Sumathi, Siang-Piao Chai , Bismuth sulphide-modified molybdenum disulphide as an efficient photocatalyst for hydrogen production under simulated solar light. The address for the corresponding author was captured as affiliation for all authors. Please check if appropriate. Catcom(2017), doi: 10.1016/j.catcom.2017.05.004

Bismuth sulphide-modified molybdenum disulphide as an efficient photocatalyst for hydrogen production under simulated solar light

W. P. Cathie Lee[a], Meei-Mei Gui[b], Lling-Lling Tan[b], Ta-Yeong Wu[a], S. Sumathi[c], Siang-Piao Chai[a*]

[a] Multidisciplinary Platform of Advanced Engineering, Chemical Engineering Discipline, School of Engineering, Monash University, Jalan Lagoon Selatan, 47500 Bandar Sunway, Selangor, Malaysia

[b] School of Engineering and Physical Sciences, Heriot-Watt University Malaysia, Jalan Venna P5/2, Precinct 5, 62200 Putrajaya, Malaysia

[c] Faculty of Engineering and Green Technology, Universiti Tunku Abdul Rahman Kampar Campus, Jalan Universiti, Bandar Barat, 31900 Kampar Perak, Malaysia

*Corresponding author:

Tel: +603-55146234; Fax: +603-55146207

E-mail address: chai.siang.piao@monash.edu

Abstract

To overcome rapid electron-hole recombination and the need for employing noble metals as co-catalysts for photocatalytic water splitting, the present work reports on the fabrication of bismuth sulphide (Bi_2S_3)-modified molybdenum disulphide (MoS_2) as an efficient hybrid photocatalyst. Under simulated solar light irradiation, the Bi_2S_3/MoS_2 photocatalyst with an optimum molar ratio of Mo to Bi of 50% (mol/mol) achieved a H_2 production rate of 61.4 μmol/h. The photocatalytic enhancement was attributed to an effective charge transfer mechanism between Bi_2S_3 and MoS_2, as evidenced by photoelectrochemical characterization. A plausible reaction mechanism over the as-prepared Bi_2S_3/MoS_2 photocatalyst was also proposed based on the experimental results obtained.

Keywords: hydrogen production; transition metal dichalcogenide; photocatalyst

1.0 Introduction

Due to population and economic growth, particularly in emerging market economies, global demand for energy is increasingly rapidly. Energy security concerns are gradually emerging as more consumers require ever more energy resources. Moreover, high consumption of fossil fuels leads to greenhouse gas emissions, particularly carbon dioxide (CO_2) which contributes to global warming. Therefore, there is an immediate need for alternative renewable fuels to reduce the dependency on fossil fuels. Among the various renewable projects to date, the photocatalytic splitting of water to generate hydrogen (H_2) fuel has garnered interdisciplinary research attention to meet the long-term worldwide energy demands without utilizing further CO_2-generating power resources [1-3]. However, the state-of-the-art technology is far from being optimal due to low overall photoconversion. Hence, breakthroughs in the preparation of efficient photocatalysts which are active under solar light, are necessary towards realizing the process for commercial applications.

Among the studied photocatalysts to date, metal sulphide semiconductors have been widely studied due to their narrow band gaps, high efficiency of light absorption and photocatalytic activity [4-7]. In particular, bismuth sulphide (Bi_2S_3) has garnered incessant research interest due to its narrow band gap of 1.3 – 1.7 eV [8-10]. However, the main drawback with any sulphur-containing catalysts is that their photoactivities are limited due to problems with photocorrosion and rapid charge recombination. Therefore, this leads to our interest in preparing heterostructured Bi_2S_3-based photocatalyst for the photocatalytic splitting of water. The general concept is to reduce rapid electron-hole recombination by merging two semiconductors with different energy levels to prolong the travel pathway of electrons.

Molybdenum disulphide (MoS_2) is a two dimensional material classified as a transition metal dichalcogenide. Previous works have shown that heterostructures of MoS_2/Bi_2S_3 are efficient for various applications such as Cr (VI) reduction [11], degradation of rhodamine B, atrazine and phenol red [12, 13]. To the best of our knowledge, there has yet to be a study on the application of Bi_2S_3/MoS_2 photocatalyst for solar H_2 generation. In this work, Bi_2S_3/MoS_2 photocatalysts were synthesized via an anion-exchange method. The photocatalytic activity of the as-synthesized photocatalyst was evaluated in the photocatalytic splitting of water under simulated solar light irradiation using Na_2S/Na_2SO_3 as sacrificial reagent. The improved performance of Bi_2S_3/MoS_2 photocatalyst in H_2 production provides a new pathway towards the goal of attaining clean renewable energy through water-splitting.

2.0 Experimental procedure

2.1 Materials

Bismuth (III) nitrate pentahydrate ($Bi(NO_3)_3{\cdot}5H_2O$), thioacetamide (C_2H_5NS), sodium molybdate ($Na_2MoO_4{\cdot}2H_2O$) were supplied by Sigma Aldrich. Sodium tungstate dehydrate ($Na_2WO_4{\cdot}5H_2O$) and ethanol were supplied from Merck and Friendemann Schmidt, respectively. All chemicals were of analytical reagent grade and were used as received without further purification. Deionized (DI) water was used in all experiments.

2.2 Synthesis of Bi_2WO_6

Bi_2WO_6 was prepared following modified methods reported from our previous work [14]. In brief, 0.4 mmol of $Na_2WO_4{\cdot}5H_2O$ first dissolved in DI water after which 0.8 mmol of $Bi(NO_3)_3{\cdot}5H_2O$ was then added into the mixture slowly to form a white solution. The mixture

was subsequently stirred for 1 h before being transferred to a Teflon lined autoclave for 15 h at 160°C. The precipitate was washed with DI water and ethanol before drying in an oven.

2.3 Synthesis of MoS_2/Bi_2S_3

For the preparation of MoS_2/Bi_2S_3 photocatalyst, a predetermined amount of $Na_2MoO_4{\cdot}2H_2O$ was dissolved in DI water before adding C_2H_5NS, the mixture was then stirred for 1 h at ambient condition. The as-prepared Bi_2WO_6 from Section 2.2 and a stoichiometric amount of C_2H_5NS were then added into the mixture with the aid of sonication to ensure a homogeneous mixture. After 1 h of sonication, the mixture was placed in a Teflon lined autoclave for 24 h at 200° C. The photocatalyst was then removed and washed with DI water and ethanol before drying in an oven. Pristine Bi_2S_3 was prepared through an in-situ anion-exchange between Bi_2WO_6 and the sulphur source under similar conditions while pristine MoS_2 was prepared following the method reported elsewhere [15]. MoS_2/Bi_2S_3 samples were prepared based on the molar ratio of Mo to Bi and were denoted as XMBS (X = 10, 30, 50 and 70 mole%).

2.4 Material characterization

The as-synthesized samples were analysed with field-emission scanning electron microscope (FE-SEM) (Hitachi SU8010) with energy dispersive X-ray (EDX) and transmission electron microscope (TEM) (TECNAI G2 F20) with an accelerating voltage of 200 kV. The X-ray diffraction (XRD) patterns of the samples prepared were determined using Bruker D8 Discover X-Ray diffractometer with CuK_α radiation (λ = 0.15406 nm) at a scan rate of 0.02 s^{-1}. The optical properties of the as-prepared samples were determined using ultraviolet-visible (UV-Vis) spectrometer (Agilent Cary 100) from 200 –800 nm. Photoluminescence (PL) measurements

were analysed using LS 55 PerkinElmer fluorescence spectrometer with the excitation wavelength of 320 nm. The emission spectra were scanned from 610 – 670 nm.

2.5 Photoelectrochemical measurements

Electrochemical impedance spectroscopy (EIS) Nyquist plots, transient photocurrent responses and Mott-Schottky plot were conducted in a three electrode electrochemical quartz cell with CHI6005E electrochemical workstation. 0.5 M Na_2SO_4 was used as the electrolyte for all photoelectrochemical measurements. Drop-casting method was employed to prepare the working electrode whereby slurry was prepared through suspension of samples in ethanol and casted onto fluorine-doped tin oxide (FTO) glass slide. The working electrode has an active area of 1 cm^2, where Pt and Ag/AgCl were used as counter and reference electrode respectively. The Mott-Schottky plots were measured from -1 to 1 V at 100 Hz frequency while transient photocurrent responses were measured with an applied bias of 0.5 V. EIS was performed over the frequency from 0.1 to 10^5 Hz with amplitude of 0.01 V.

2.6 Evaluation of photocatalytic activity

The photocatalytic water splitting experiments were conducted at ambient pressure and temperature. MoS_2/Bi_2S_3 (10 mg) was dispersed in 120 mL DI water containing 0.5 M Na_2S and 0.5 M Na_2SO_3 which act as sacrificial reagents. The H_2 production was carried out under the irradiation of 500 W Xe lamp fitted with AM1.5 filter to simulate the solar light spectrum. The product gas was analysed using an online gas chromatography.

3.0 Results and discussion

3.1 Structural and chemical characterization

The crystallographic structures of the as-synthesized photocatalysts were characterised using XRD (see Figure S1). As shown in Figure S1(a), the peaks observed in the diffraction pattern of pristine Bi_2S_3 corresponded to the orthorhombic structure of Bi_2S_3 (JCPDS #017-0320), which verified the successful synthesis of Bi_2S_3. Comparing the diffraction patterns of Bi_2S_3 (Figure S1(a)) and Bi_2WO_6 (Figure S1(g)), an additional distinct peak at 55.8^o was observed for the latter (JCPDS# 039-0256). This unique peak corresponding to Bi_2WO_6 was not observed in other samples as shown in Figure S1(b – e), confirming the formation of Bi_2S_3 from Bi_2WO_6. Furthermore, the peak observed at 14.4 ° (marked #) in Figure S1(b – e) can be ascribed to the (002) facet of MoS_2. In addition, the peaks presented in Figure S1(f) are also in accordance with the hexagonal crystal structure of MoS_2 (JCPDS# 037-1492) [16, 17].

XPS was performed to analyse the surface chemical state of pristine Bi_2S_3 and 50MBS (see Figure 1 and Figure S2). As shown in Figure S2(A), the survey scan of 50MBS revealed the presence of elements Bi and Mo. The representative Bi core level XPS spectrum depicted in Figure 1(A) showed two peaks centered at 158.7 eV and 164.0 eV, which were indexed to Bi $4f_{7/1}$ and Bi $4f_{5/2}$ respectively. This indicated that Bi existed mainly in the chemical state of +3 [18]. Figure 1(B) shows the high resolution XPS spectrum for Mo. The binding energies of 235.6 eV and 232.4 eV corresponded to Mo $3d_{3/2}$ and Mo $3d_{5/2}$ respectively [6, 19]. The results obtained were in agreement with the XRD results presented in Figure S1. The characteristic peaks for S could be observed at 225.8 eV and 161.4 eV. It is to note that W^{6+} peaks at 35.8 and 37.9 eV, corresponding to W $4f_{7/2}$ and W $4f_{5/2}$ respectively, could not be observed in the survey

scan of Bi_2S_3 (Figure S2(B)), further confirming that Bi_2WO_6 were transformed into Bi_2S_3 [14]. The elemental scan for Bi of Bi_2S_3 sample is shown in Figure S2(C).

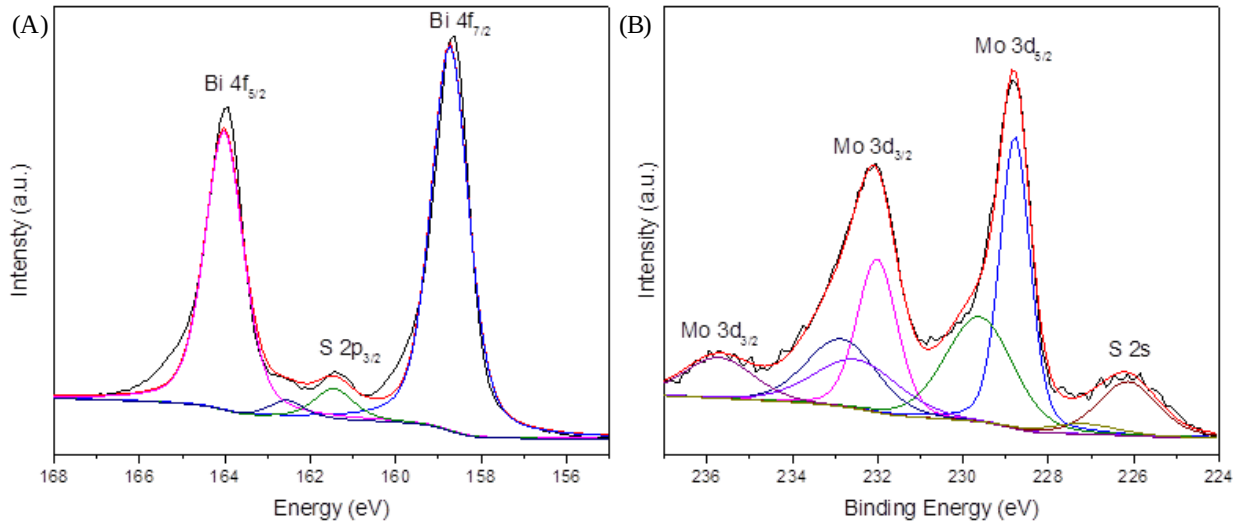

Figure 1: High resolution XPS of (A) Bi4f and (B) Mo 3d spectra of 50MBS.

The surface morphologies and structures of the photocatalysts were studied using FE-SEM and HR-TEM. Figure S3(A) shows the typical 2D structure of Bi_2WO_6 which is generally square in shape. After the anion-exchange reaction, Bi_2WO_6 transformed to Bi_2S_3 as shown in Figure S3 (B). It could be observed that Bi_2S_3 formed a rod-like structure and self-assembled into a disc with an average width of 2 µm. Owing to the lower solubility of Bi_2S_3 ($K_{sp} = 1 \times 10^{-97}$), the conversion of Bi_2WO_6 into Bi_2S_3 was easily achieved through the reaction with S^{2-} ions generated from thioacetamide [20, 21]. Figure S3(C) shows the FE-SEM image of 50MBS at high magnifications. MoS_2 nanosheets could be seen to have formed onto the surface of Bi_2S_3, where it acted as a sacrificial site for nucleation and crystallization. Figure S3(D) shows the TEM image of 50MBS. At higher magnification (inset), a lattice spacing of 0.27 nm which corresponded to the MoS_2 (100) facet could be observed. Figure S4 shows the elemental mapping pattern of Bi, Mo and S with EDX spectrum for 50MBS.

3.2 Photocatalytic water splitting to produce H_2

The photocatalytic water splitting experiments were conducted over the as-prepared photocatalysts (see Figure 2). Despite being an effective light absorption material, MoS_2 was shown to be inactive in the production of H_2. This could be attributed to the poor electrical conductivity of MoS_2, which resulted in a high recombination rate of photogenerated charge carriers [22]. In addition, Bi_2S_3 exhibited relatively low photoactivity towards water splitting, achieving a H_2 production rate of only 38.6 μmol/h. By combining MoS_2 and Bi_2S_3, the rate of H_2 generation over 10MBS hybrid photocatalyst was shown to have risen by 22% to 47.0 μmol/h. By increasing the amount of MoS_2 in the binary heterostructure, the H_2 production rate gradually increased until it reached an optimum production rate of 61.4 μmol/g.h at 50 mole% MoS_2 loading. However, a further increase in MoS_2 loading led to a reduction in H_2 production rate. This could be due to the crippling of photogenerated electron transfer between Bi_2S_3 and MoS_2 at the presence of excessive MoS_2. In contrast, when the MoS_2 content is too low, there could be inadequate light absorption to promote the excitation of electrons. Therefore, there exists an optimum loading of MoS_2 in the binary composite to achieve most efficient photocatalytic performances. The stability performance of 50MBS was evaluated by subjecting it to 4 consecutive photocatalytic runs under the same reaction condition. The results showed that 50MBS retained almost 90% of its reactivity after its forth cycle (Figure S5).

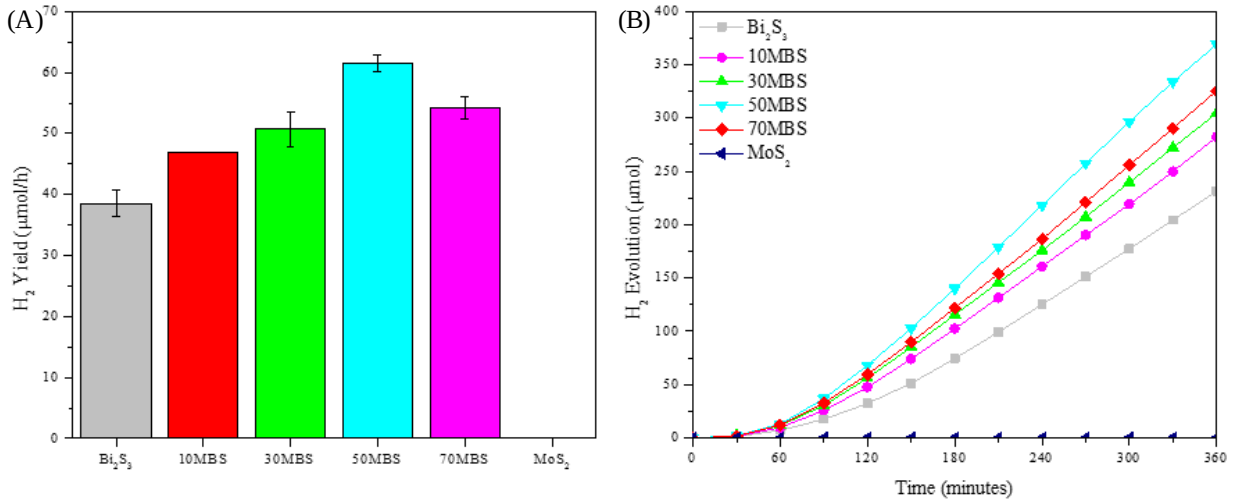

Figure 2: (A) Photocatalytic H_2 production activities and (B) amount of H_2 evolved over 6 h.

3.3 Photocatalytic mechanism over Bi_2S_3/MoS_2 hybrid photocatalyst

To fully elucidate the underlying photocatalytic reaction mechanism of Bi_2S_3/MoS_2 hybrid photocatalyst, the energy structure of Bi_2S_3 and MoS_2 was studied. Firstly, the absorption band energies of Bi_2S_3 and MoS_2 were determined through diffuse reflectance spectra by the modified Tauc plot (see Figure S6(B)). The band energies for Bi_2S_3 and MoS_2 were shown to be 1.20 and 1.38 eV respectively. The Mott-Schottky plot in Figure S6(D) revealed a conduction band potential of approximately –0.5 V/NHE and 0.0 V/NHE for MoS_2 and Bi_2S_3, respectively. Based on the obtained results, a band position diagram for the hybrid photocatalyst was proposed (Figure 3). As the conduction band of MoS_2 is more negative than Bi_2S_3, the diagram resembled a type-II band alignment structure. Upon light irradiation, photoinduced electrons migrated from MoS_2 to Bi_2S_3, thus enhancing the charge separation process. The PL spectrum shown in Figure S6(C) indicated that pristine Bi_2S_3 suffered from high charge recombination rate. The lower peak intensity for the Bi_2S_3/MoS_2 hybrid confirmed a prolonged electron-hole separation rate.

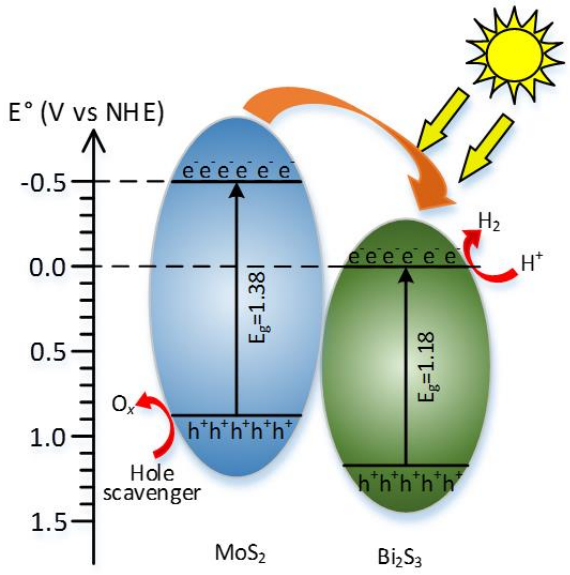

Figure 3: Charge transfer mechanism of MoS_2/Bi_2S_3.

A useful tool to gauge the separation efficiency and lifetime of photogenerated charge carriers can be measured by the transient photocurrent response [23, 24]. Figure 4(A) shows the transient photocurrent responses for 50MBS and Bi_2S_3. 50MBS demonstrated a higher photocurrent density as compared to Bi_2S_3, which showed a rapid decrease in photocurrent density over 20 seconds upon simulated solar light irradiation. The observed phenomenon indicated that the addition of MoS_2 reduced the electron-hole pair recombination rate and extended the activity of charge carriers. Electrochemical impedance spectroscopy Nyquist plot was employed to further investigate the transfer of photogenerated charge carriers as shown in Figure 4(B). A smaller semi-arc shown by 50MBS, under the irradiation of simulated solar light, indicated the decrease in charge transfer resistance and the solid state interface layer resistance on the surface of 50MBS [25]. This signifies that 50MBS has a more efficient charge transfer interface as compared to Bi_2S_3. These findings further solidify the importance of MoS_2 for enhanced photoactivity.

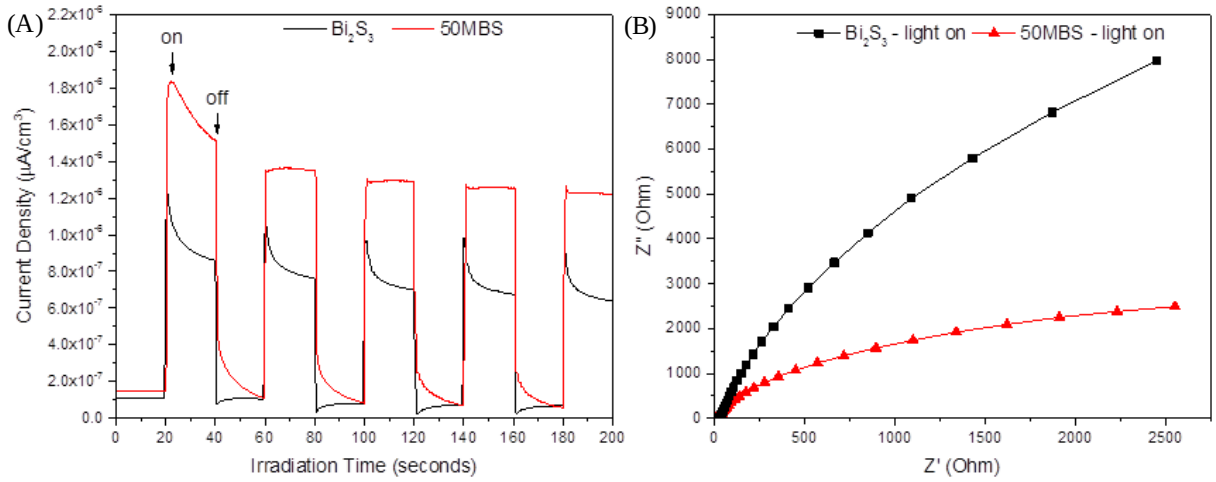

Figure 4: (A) Photocurrent responses of Bi_2S_3 and 50MBS and (B) electrochemical impedance spectroscopy of Bi_2S_3 and 50MBS.

4.0 Conclusions

In conclusion, a noble metal-free MoS_2 modified Bi_2S_3 photocatalyst was successfully synthesized through an anion exchange method. To the best of our knowledge, this is the first report on the use of Bi_2S_3/MoS_2 photocatalyst for the photocatalytic production of H_2. At the optimum of 50% Mo:Bi (mol/mol), the H_2 evolution rate was determined to be 61.4 μmol/h under simulated solar light, which was more than 50% higher as compared to pristine Bi_2S_3 (38.6 μmol/h). The enhancement in photoactivity was ascribed to the intimate interface contact between Bi_2S_3 and MoS_2, which improved the separation of electron-hole pairs. The findings from this work could potentially bring photocatalytic water splitting one step closer to the realization of clean and carbon emission-free energy for the future.

Acknowledgements

This work is financially supported by Ministry of Science, Technology and Innovation (MOSTI) Malaysia for providing the financial support under e-science Fund (Ref. no. 03-02-10SF0244).

References

[1] K. Chang, X. Hai, J. Ye, Transition Metal Disulfides as Noble-Metal-Alternative Co-Catalysts for Solar Hydrogen Production, Advanced Energy Materials, 6 (2016) 1502555.
[2] Y. Horiuchi, T. Toyao, K. Miyahara, L. Zakary, D.D. Van, Y. Kamata, T.-H. Kim, S.W. Lee, M. Matsuoka, Visible-light-driven photocatalytic water oxidation catalysed by iron-based metal-organic frameworks, Chemical Communications, 52 (2016) 5190-5193.
[3] T.W. Woolerton, S. Sheard, E. Reisner, E. Pierce, S.W. Ragsdale, F.A. Armstrong, Efficient and Clean Photoreduction of CO_2 to CO by Enzyme-Modified TiO_2 Nanoparticles Using Visible Light, Journal of the American Chemical Society, 132 (2010) 2132-2133.
[4] T. Saison, P. Gras, N. Chemin, C. Chanéac, O. Durupthy, V. Brezová, C. Colbeau-Justin, J.-P. Jolivet, New Insights into Bi_2WO_6 Properties as a Visible-Light Photocatalyst, The Journal of Physical Chemistry C, 117 (2013) 22656-22666.
[5] J. Tian, Y. Sang, G. Yu, H. Jiang, X. Mu, H. Liu, A Bi_2WO_6-Based Hybrid Photocatalyst with Broad Spectrum Photocatalytic Properties under UV, Visible, and Near-Infrared Irradiation, Advanced Materials, 25 (2013) 5075-5080.
[6] W. Zhou, Z. Yin, Y. Du, X. Huang, Z. Zeng, Z. Fan, H. Liu, J. Wang, H. Zhang, Synthesis of Few-Layer MoS_2 Nanosheet-Coated TiO_2 Nanobelt Heterostructures for Enhanced Photocatalytic Activities, Small, 9 (2013) 140-147.
[7] X. Gao, H.B. Wu, L. Zheng, Y. Zhong, Y. Hu, X.W. Lou, Formation of Mesoporous Heterostructured $BiVO_4/Bi_2S_3$ Hollow Discoids with Enhanced Photoactivity, Angewandte Chemie, 126 (2014) 6027-6031.
[8] L. Li, N. Sun, Y. Huang, Y. Qin, N. Zhao, J. Gao, M. Li, H. Zhou, L. Qi, Topotactic Transformation of Single-Crystalline Precursor Discs into Disc-Like Bi_2S_3 Nanorod Networks, Advanced Functional Materials, 18 (2008) 1194-1201.
[9] Z.-Q. Liu, W.-Y. Huang, Y.-M. Zhang, Y.-X. Tong, Facile hydrothermal synthesis of Bi_2S_3 spheres and CuS/Bi_2S_3 composites nanostructures with enhanced visible-light photocatalytic performances, CrystEngComm, 14 (2012) 8261-8267.
[10] Li, B., Y. Zhang, R. Du, L. Gan, and X. Yu, Synthesis of Bi_2S_3–Au Dumbbell Heteronanostructures with Enhanced Photocatalytic and Photoresponse Properties. Langmuir, 2016. 32(44): 11639-11645.
[11] B. Weng, X. Zhang, N. Zhang, Z.-R. Tang, Y.-J. Xu, Two-Dimensional MoS_2 Nanosheet-Coated Bi_2S_3 Discoids: Synthesis, Formation Mechanism, and Photocatalytic Application, Langmuir, 31 (2015) 4314-4322.
[12] L.-L. Long, J.-J. Chen, X. Zhang, A.-Y. Zhang, Y.-X. Huang, Q. Rong, H.-Q. Yu, Layer-controlled growth of MoS_2 on self-assembled flower-like Bi_2S_3 for enhanced photocatalysis under visible light irradiation, NPG Asia Mater, 8 (2016) e263.
[13] S.V.P. Vattikuti, C. Byon, Bi_2S_3 nanorods embedded with MoS_2 nanosheets composite for photodegradation of phenol red under visible light irradiation, Superlattices and Microstructures, 100 (2016) 514-525.
[14] X.Y. Kong, Y.Y. Choo, S.-P. Chai, A.K. Soh, A.R. Mohamed, Oxygen vacancy induced Bi_2WO_6 for the realization of photocatalytic CO_2 reduction over the full solar spectrum: from the UV to the NIR region, Chemical Communications, 52 (2016) 14242-14245.
[15] Lee, W.P.C., F.-H. Wong, N.K. Attenborough, X.Y. Kong, L.-L. Tan, S. Sumathi, and S.-P. Chai, Two-dimensional bismuth oxybromide coupled with molybdenum disulphide for enhanced

dye degradation using low power energy-saving light bulb. Journal of Environmental Management, 2017. 197 63-69.
[16] Wang, X., M. Hong, F. Zhang, Z. Zhuang, and Y. Yu, Recyclable Nanoscale Zero Valent Iron Doped g-C_3N_4/MoS_2 for Efficient Photocatalysis of RhB and Cr(VI) Driven by Visible Light. ACS Sustainable Chemistry & Engineering, 2016. 4(7) 4055-4063.
[17] C. Zhai, M. Sun, M. Zhu, K. Zhang, Y. Du, Insights into photo-activated electrode for boosting electrocatalytic methanol oxidation based on ultrathin MoS_2 nanosheets enwrapped CdS nanowires. International Journal of Hydrogen Energy, 2017. 42(8) 5006-5015.
[18] L.-X. Hao, G. Chen, Y.-G. Yu, Y.-S. Zhou, Z.-H. Han, Y. Liu, Sonochemistry synthesis of Bi_2S_3/CdS heterostructure with enhanced performance for photocatalytic hydrogen evolution, International Journal of Hydrogen Energy, 39 (2014) 14479-14486.
[19] J. Xu, X. Cao, Characterization and mechanism of MoS_2/CdS composite photocatalyst used for hydrogen production from water splitting under visible light, Chemical Engineering Journal, 260 (2015) 642-648.
[20] Z. Zhang, W. Wang, L. Wang, S. Sun, Enhancement of Visible-Light Photocatalysis by Coupling with Narrow-Band-Gap Semiconductor: A Case Study on Bi_2S_3/Bi_2WO_6, ACS Applied Materials & Interfaces, 4 (2012) 593-597.
[21] H. Cheng, B. Huang, Y. Liu, Z. Wang, X. Qin, X. Zhang, Y. Dai, An anion exchange approach to Bi_2WO_6 hollow microspheres with efficient visible light photocatalytic reduction of CO2 to methanol, Chemical Communications, 48 (2012) 9729-9731.
[22] K. Chang, Z. Mei, T. Wang, Q. Kang, S. Ouyang, J. Ye, MoS_2/Graphene Cocatalyst for Efficient Photocatalytic H_2 Evolution under Visible Light Irradiation, ACS Nano, 8 (2014) 7078-7087.
[23] F.-X. Xiao, J. Miao, B. Liu, Self-assembly of aligned rutile@anatase TiO_2 nanorod@CdS quantum dots ternary core-shell heterostructure: cascade electron transfer by interfacial design, Materials Horizons, 1 (2014) 259-263.
[24] J. Xie, J. Zhang, S. Li, F. Grote, X. Zhang, H. Zhang, R. Wang, Y. Lei, B. Pan, Y. Xie, Controllable Disorder Engineering in Oxygen-Incorporated MoS_2 Ultrathin Nanosheets for Efficient Hydrogen Evolution, Journal of the American Chemical Society, 135 (2013) 17881-17888.
[24] Y. Zhang, Y. Zhu, J. Yu, D. Yang, T.W. Ng, P.K. Wong, J.C. Yu, Enhanced photocatalytic water disinfection properties of Bi_2MoO_6-RGO nanocomposites under visible light irradiation, Nanoscale, 5 (2013) 6307-6310.

Highlights

- Bi_2S_3 modified MoS_2 as a highly efficient hybrid photocatalyst under simulated sunlight
- Optimum loading 50% Mo:Bi molar ratio with H_2 production rate of 61.4 µmol/h
- Improved H_2 production due to effective charge transfer between Bi_2S_3 and MoS_2